© 2015. Published by The Company of Biologists Ltd | Development (2015) 142, 1794-1805 doi:10.1242/dev.118372

RESEARCH ARTICLE

A cellular process that includes asymmetric cytokinesis remodels the dorsal tracheal branches in *Drosophila* larvae

Alexandru Stefan Denes, Oguz Kanca and Markus Affolter*

ABSTRACT

Tubular networks are central to the structure and function of many organs, such as the vertebrate lungs or the *Drosophila* tracheal system. Their component epithelial cells are able to proliferate and to undergo complex morphogenetic movements, while maintaining their barrier function. Little is known about the details of the mitotic process in tubular epithelia. Our study presents a comprehensive model of cellular remodeling and proliferation in the dorsal branches of third-instar *Drosophila* larvae. Through a combination of immunostaining and novel live imaging techniques, we identify the key steps in the transition from a unicellular to a multicellular tube. Junctional remodeling precedes mitosis and, as the cells divide, new junctions are formed through several variations of what we refer to as 'asymmetric cytokinesis'. Depending on the spacing of cells along the dorsal branch, mitosis can occur either before or after the transition to a multicellular tube. In both instances, cell separation is accomplished through asymmetric cytokinesis, a process that is initiated by the ingression of the cytokinetic ring. Unequal cell compartments are a possible but rare outcome of completing mitosis through this mechanism. We also found that the Dpp signaling pathway is required but not sufficient for cell division in the dorsal branches.

KEY WORDS: *Drosophila*, Tracheal remodeling, Asymmetric cytokinesis, Live imaging, Actomyosin

INTRODUCTION

Tubular structures are ubiquitous across animal phyla, and in many cases they form branched continuous epithelial or endothelial networks. At the cellular level, most tubes have the shape of a wrapped epithelial sheet that encloses a lumen on the apical side. The integrity and impermeability of the tube walls is maintained through adherens junctions (AJs) and septate junctions (SJs), while the lumen is supported by pressure and occasionally by a secreted apical extracellular matrix. Although mitosis in isolated, single cells is a well-understood process (Harris and Tepass, 2010), less is known about cell division within flat or tubular epithelia, where the forces generated by the actomyosin cortex are balanced by E-Cadherin-mediated intercellular adhesion (Bourdages and Maddox, 2013). The cells within epithelial sheets must undergo divisions and rearrangements without disrupting the intercellular junctions that are necessary for barrier function (Blanpain and Fuchs, 2009). Tissue homeostasis and injury repair require morphogenetic movements similar to those in early development (Martin and Parkhurst, 2004) as well as specialized stem cells (Giangreco et al., 2009; Rock and Hogan, 2011). Several recent studies (Founounou et al., 2013; Guillot and Lecuit, 2013; Herszterg et al., 2013) have highlighted the dynamic reorganization of AJs during cytokinesis in the epithelia of *Drosophila* embryos (Guillot and Lecuit, 2013) and the *Drosophila* pupal notum epithelium (Founounou et al., 2013; Herszterg et al., 2013). The actomyosin ring that drives cytokinesis deforms the AJ of the neighboring cells, detaching from them once the tension exceeds a certain threshold (Founounou et al., 2013; Guillot and Lecuit, 2013). As shown by laser ablation and genetic experiments, the tensile stress in the surrounding cells also influences the geometry of the emerging junction in a non-autonomous manner (Herszterg et al., 2013).

The *Drosophila* tracheal system is one of the established models for the study of branched tubular epithelial networks (Ghabrial et al., 2003; Affolter and Caussinus, 2008). Depending on their diameter, tracheal branches may alternatively be multicellular, unicellular or subcellular tubes (Uv et al., 2003); this diversity makes them well suited for the study of tubulogenesis and epithelial morphogenesis. The embryonic tracheal system starts to develop in a segmental fashion as ten invaginating placodes on either side of the embryo. From an invaginated sac-like structure, several primary sprouts grow out, subsequently leading to the formation of secondary and terminal branches in a tightly regulated sequence (Samakovlis et al., 1996; Ghabrial et al., 2003; Uv et al., 2003). Each hemisegment contains a basic unit called tracheomere, consisting of the dorsal trunk (DT) and six other branches (Fig. 1A). Tracheomeres are connected to their neighbors along the anteroposterior axis by specialized fusion cells (Tanaka-Matakatsu et al., 1996), and within each hemisegment, the left-side dorsal branch (DB) connects with its right-side counterpart. Branchless (Bnl)/FGF signaling is crucially involved at all stages of tracheal development, including the initial budding, primary, secondary and terminal branching (Sutherland et al., 1996), air sac primordium (ASP) induction (Sato and Kornberg, 2002) and pupal abdominal trachea (PAT) migration (Chen and Krasnow, 2014). The elongation of the dorsal branch does not occur in the absence of Dpp signaling (Chen et al., 1998), because, by itself, Bnl/FGF only induces filopodial extensions (Ribeiro et al., 2002). Dpp signaling is required to suppress Spalt (Sal) in the DBs, enabling the formation of a unicellular tube through cell intercalation (Ribeiro et al., 2004; Neumann and Affolter, 2006).

Most studies have focused on the embryonic tracheal system, partly because it is easily accessible to live imaging. The tracheal system of *Drosophila* larvae displays a set of characteristics that sets it apart from other models of tubulogenesis. In common with most larval tissues, the cells of the tracheal system grow in size by endoreplicating their DNA (becoming polyploid) and are largely replaced during the pupal stage (Manning and Krasnow, 1993; Edgar and Orr-Weaver, 2001). However, specific regions

Biozentrum, University of Basel, Klingelbergstrasse 50/70, Basel CH 4056, Switzerland.

*Author for correspondence (markus.affolter@unibas.ch)

Received 3 October 2014; Accepted 23 March 2015

Development (2015) 142, 1794-1805 doi:10.1242/dev.118372

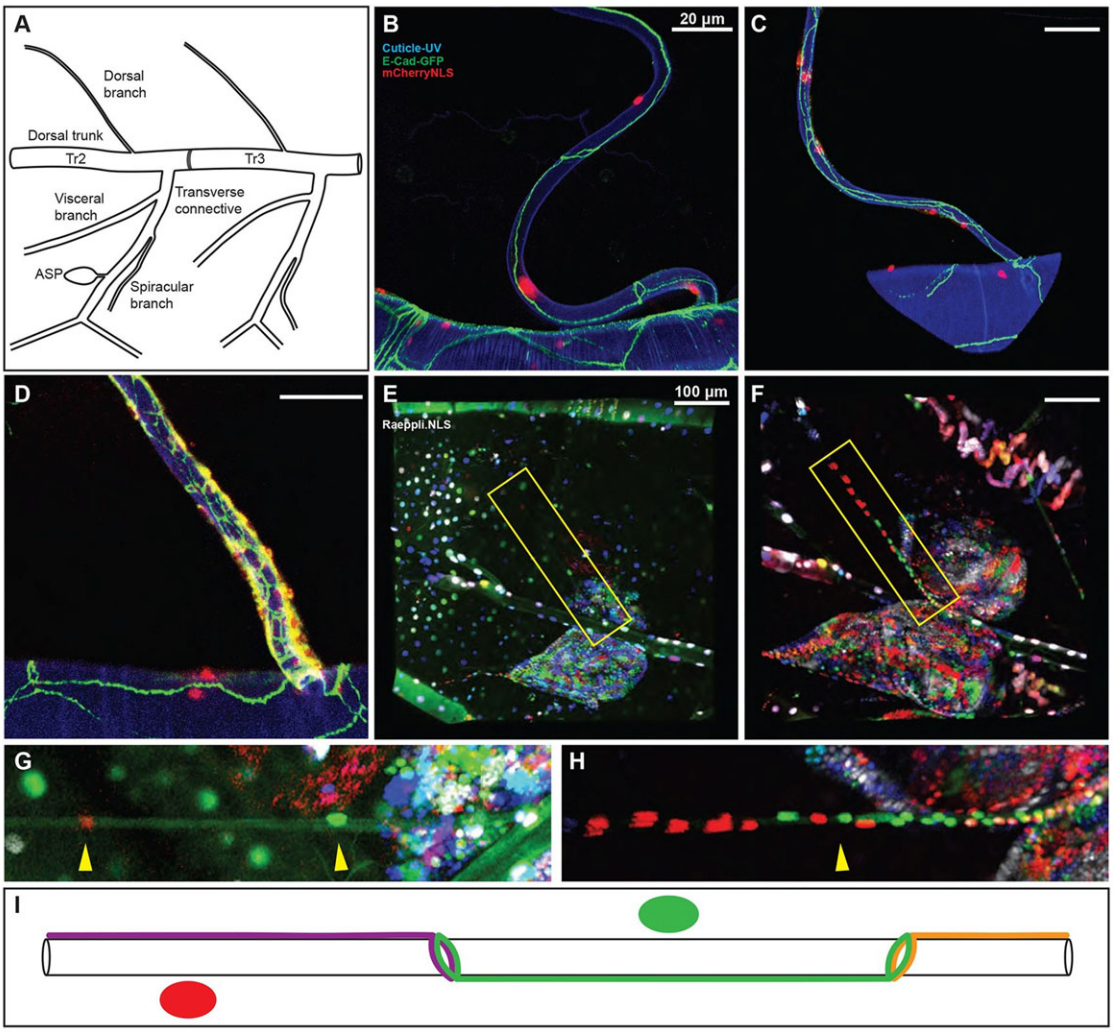

Fig. 1. The dorsal branches of *Drosophila* larvae undergo several rounds of cell division and junctional rearrangements. (A) Schematic representation of the second and third tracheal metameres. (B-D) Dissected trachea from *E-Cad-GFP; blt-mCherryNLS* larvae, stained with anti-GFP/A488 (green); the lumen is highlighted by cuticle autofluorescence in the UV channel (blue). (B) The basic architecture of the dorsal branches, a unicellular tube with autocellular junctions, is retained from the embryonic stage into early L3. (C) DB cells divide within about 24 h and the branches reorganize into multicellular tubes. (D) Highly remodeled branch from the WL stage, ~48 h after hatching into the third instar. (E,F) Third instar larva (*tub-Gal80^{ts}/Raeppli.NLS53D; actin-Gal4, UAS-Flp/Raeppli.NLS89A*) sequentially imaged approximately 1 day apart. The following color code was used for the fluorescent proteins: green (TagBFP), gray (mTFP1), blue (E2-Orange) and red (mKate2). (G,H) Magnified insets from the yellow boxed regions of E,F. (G) Neighboring nuclei that express different fluorescent proteins (yellow arrowheads). (H) Mixing between the red and green clonal populations along the axis of the lumen (yellow arrowhead). (I) The position of DB nuclei and junctions before remodeling.

of the tracheal system, i.e. the entire Tr2 (where the ASP originates), the dorsal branches (DBs) of Tr3-Tr5 and all the spiracular branches (SBs), were found to retain their proliferative potential (Guha and Kornberg, 2005; Guha et al., 2008; Sato et al., 2008; Weaver and Krasnow, 2008; Pitsouli and Perrimon, 2010). Although some populations of polyploid cells have been shown to re-enter the mitotic cycle (Fox et al., 2010), the cells that the DBs and SBs comprise are likely diploid cells, and functionally similar to those in the imaginal disks (Sato et al., 2008; Weaver and Krasnow, 2008; Djabrayan et al., 2014).

We have previously studied how the coordinated action of cell signaling and cell migration leads to dorsal branch formation during embryogenesis [reviewed by Affolter and Caussinus (2008); Maruyama and Andrew (2012)]. Here, we investigate dorsal branch remodeling during larval development, a dynamic cellular process that includes mitosis, unlike the rearrangement of the embryonic dorsal branches.

RESULTS

Progression of remodeling in the dorsal branches during the third instar

The tracheal system of the early third instar larva is very similar to that of the preceding L2 stage, aside from changes in the branching structure of the anterior spiracles and the expansion of the DT lumen. As previously shown (Weaver and Krasnow, 2008), the cells in the dorsal branches of the anterior tracheomeres (Tr2 to Tr5) are able to proliferate, similar to the cells from the spiracular branches (Pitsouli and Perrimon, 2010). During early L3, the autocellular junctions that were established in the embryonic stage through cell intercalation (Ribeiro et al., 2004) are still apparent (Fig. 1B,I). However, within about 24 h, the DBs transform into multicellular

Development (2015) 142, 1794-1805 doi:10.1242/dev.118372

tubes (Fig. 1C), the cellular complexity of which continues to increase until the wandering larva (WL) stage (Fig. 1D).

In order to gain an overview of tracheal remodeling at the cellular level, we made use of Raeppli, a novel technique for cell labeling based on the differential expression of four spectrally separable fluorescent proteins (Kanca et al., 2014). We used two copies of Raeppli for a stronger signal and a broader color palette, under the control of the *Tub-Gal80^{ts};UAS-Flp,Act-Gal4* induction system (Kanca et al., 2014). The animals were first reared at 18°C until L2 stage and were then transferred to the non-permissive temperature of 29°C, unlocking Raeppli and irreversibly forcing a stochastic color selection for each copy of the Raeppli construct. After staging, the L3 larvae were imaged twice, at 20 and 48 h, respectively, using cold anesthesia (supplementary material Fig. S1) to suppress their movements during image acquisition (Fig. 1E,F). The neighboring red- and green-labeled cells (Fig. 1G, yellow arrows) had undergone three or four rounds of division between the imaging sessions, consistent with a cell cycle of ∼8 h (Fig. 1E,F). At first glance, the narrow and elongated shape of the DB cells would seem to favor a 'sausage-chain' mode of cell division that would produce largely non-overlapping clonal populations. Instead, we observed a considerable degree of overlap between the two labeled populations (Fig. 1H, yellow arrow).

Junctional remodeling and mitosis occur in parallel in the dorsal branches

Dorsal branch cells show a peculiar architecture, acquired through cell intercalation in the embryo. The cells are long, thin, wrapped around the lumen and sealed by a long autocellular AJ (Fig. 1B). Puzzled by the ability of tube cells to divide, we wanted to study their behavior in detail and with high spatial resolution during mitosis. We observed a shortening of the autocellular junctions in the DBs and a corresponding lengthening of the intercellular junctions (Fig. 2A,B) before mitosis was initiated. This cellular behavior, which we will refer to as junctional remodeling, resembles the embryonic intercalation process, albeit in the opposite direction. Along the entire length of a dorsal branch, the cells expanded their intercellular junctions, with those closer to the DT progressing at a faster pace than those closer to the terminal cell (data not shown). Unlike in the embryonic tracheal system, where the migration of the tip cell is a major driving force for the intercalation process (Caussinus et al., 2008), the stalk cells in the larval DBs do not move relative to the DT or the terminal cell, so the junctional remodeling process is likely cell autonomous.

We have investigated the position and structure of the intercellular AJs during the remodeling process, using a functional GFP knock-in version of DE-Cadherin (Huang et al., 2009) in combination with an antibody against Dlg, a component of the septate junctions that is localized to the basolateral side. The position of the nuclei was visualized with *btl-mCherryNLS*, and for increased sensitivity we also performed anti-GFP antibody staining. Surprisingly, DE-Cadherin was found to be concentrated in two belts: a primary one at the apical side of the cell, likely part of the AJ; and an additional one in a region more basal than the septate junctions, where Dlg is localized (supplementary material Fig. S2A). The second belt of DE-Cadherin was especially prominent in the DTs, whereas in the DBs it usually appeared as a row of punctae (supplementary material Fig. S2C,C′). This distinctive 'sandwich' pattern of DE-Cadherin and Dlg was discernable throughout the tracheal system, including the fusion cells (supplementary material Fig. S2A), but was not apparent in other tissues, such as the larval epithelium or the wing disk (data not shown). We examined staged 20-28 h L3 larvae, when the first round of cell division takes place in the DBs. Although in all cases junctional remodeling preceded cell division, we identified three distinct pathways for cytokinesis.

Timing of mitosis initiation leads to differences in cytokinesis

The most common form, henceforth 'type 1', takes place after the disappearance of the autocellular junctions (Fig. 2C,D). By contrast, 'type 2' cytokinesis occurs in cells that have retained part of their self-junction (Fig. 2E-G). Finally, we refer to those rare events where the dividing cell is separated into unequal compartments as 'type 3' cytokinesis (Fig. 2H,I,O). We found that during the transition to a multicellular tube, the intercellular junctions flanking the autocellular junction elongated until they made contact, unzipping the self-junction until it completely disappeared. A new intercellular junction developed at the site, with an orthogonal orientation to the former autocellular junction. Therefore, along most of their length, DBs transitioned from a unicellular to a multicellular tube through extensive junctional rearrangement. The *de novo* intercellular junctions that separated the two daughter cells developed on the opposite side of the lumen, with respect to the position of the former autocellular junctions (Fig. 2P). Therefore, the nuclei of the newly remodeled branch ended up in pairs, with a zigzag arrangement along the length of the tube (Fig. 2D,P). Owing to this geometry, the uppermost daughter cell on the right and the lowermost daughter cell on the left arrived at a similar height and on opposite sides of the lumen (Fig. 2D). This process can explain the clonal overlap observed in the Raeppli experiments (Fig. 1H).

Type 2 cytokinesis refers to the formation of a *de novo* junction with the shape of a circumlumenal ring, within a cell that has retained part of its autocellular junction (Fig. 2F,G). During mitosis the nuclei adopted a rounded shape (Fig. 2Q′,S1) and closely associated with one side of the autocellular junction (Fig. 2Q′). Unlike in epithelial cytokinesis, the presence of a rigid apical side imposed restrictions on the range of possible cellular movements, as the forces generated by cell division were not sufficient to deform the lumen. The adherens junctions of epithelial cells are known to furrow towards the centrally positioned actomyosin ring (Bourdages and Maddox, 2013). However, the self-junction of a unicellular tube may only furrow in one direction without compromising epithelial integrity. The rounded prophase nucleus has a diameter close to that of the lumen (Fig. 2R′,S1), so it was able to approach only one side of the junction. This naturally emerging asymmetry ensured that the furrowing of the membrane and the growth of the new junction separated the daughter nuclei (Fig. 2E,L).

Type 3 cytokinesis (Fig. 2H,I) is a subtype of type 2 cytokinesis that leads to faulty abscission. The position of the nuclei relative to the intercellular junctions varies dynamically along the DB, depending on the length of the cells. Because of the smaller distances that were involved, the shorter cells completed the transition from autocellular junctions to intercellular ones faster than the longer cells. Incorrect abscission was observed when the nucleus from a longer cell was close to the intercellular junction with a shorter cell (Fig. 2H). During type 2 cytokinesis, the daughter nuclei remained aligned on one side of the autocellular junction (Fig. 2Q,Q′). By contrast, the daughter nuclei of cells undergoing type 3 cytokinesis were pushed out of alignment (Fig. 2R′,S4,S5) by the ongoing junctional remodeling (Fig. 2I). We could not pursue the ultimate fate of the bi-nucleated cells. However, as most larval tracheal cells are naturally polyploid, we assume they can remain functional. The anucleated compartments were very small compared with the other DB cells, so they probably do not

Development (2015) 142, 1794-1805 doi:10.1242/dev.118372

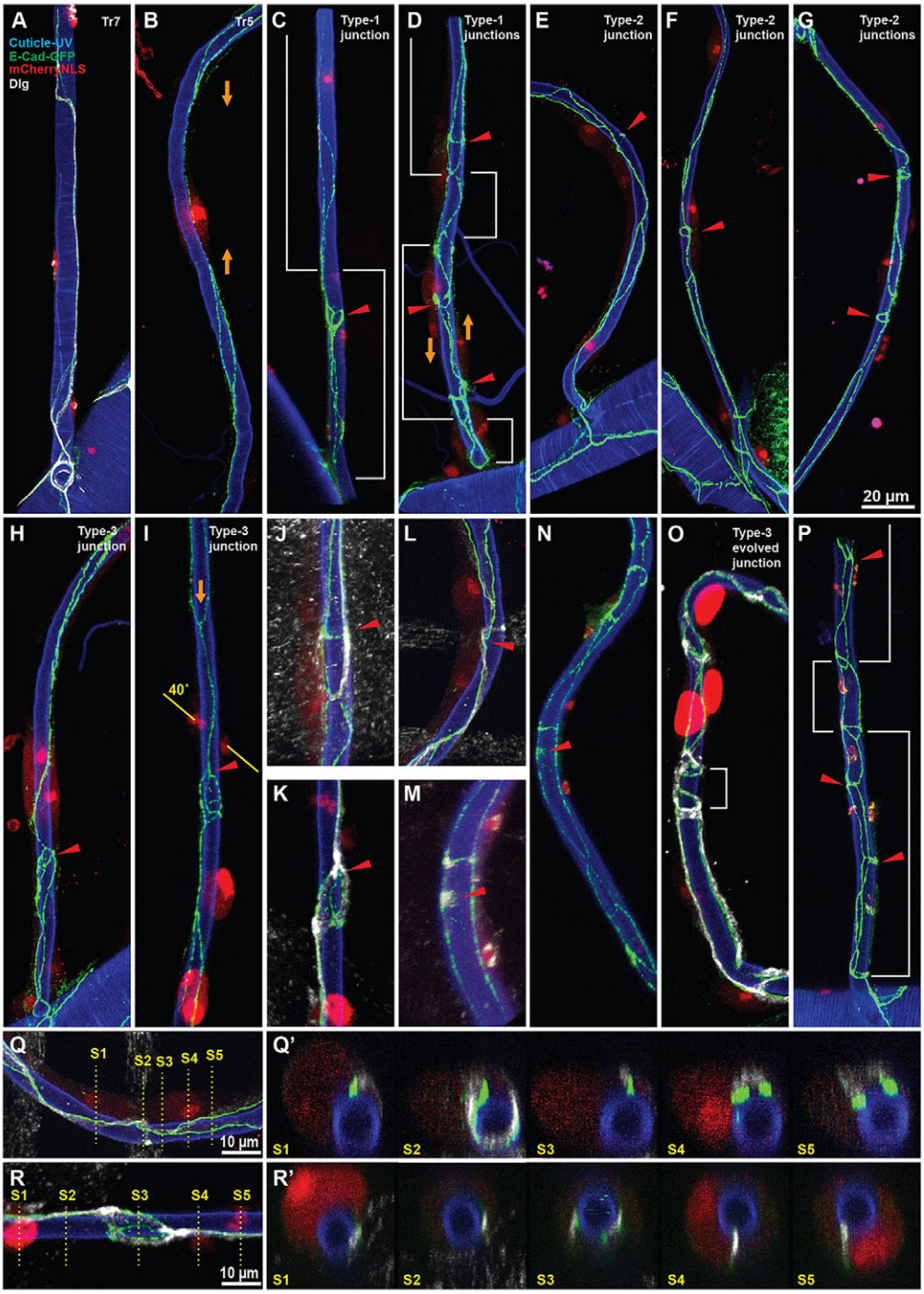

Fig. 2. Cytokinesis in the dorsal branches can take place before or after the tube becomes multicellular. (A-R) Dorsal branches from dissected *E-Cad-GFP, btl-mCherryNLS* larvae, showing cuticle autofluorescence (blue), stained with anti-GFP/A488 (green) and anti-Dlg/A633 (white). (A) Tr7 DB showing non-remodeled embryonic-type junctions 24 h into L3. (B) Tr5 DB with shortened autocellular junctions and elongated intercellular junctions (orange arrows) 24 h into L3. (C) Type 1 cytokinesis showing a new junction (red arrowhead) close to the contact between neighboring cells (white brackets). (D) Type 1 cytokinesis showing three new junctions (red arrows), with the borders between cells indicated by white brackets. Cell intercalation along the axis of the lumen (orange arrows). (E) Type 2 cytokinesis showing an incomplete circumlumenal junction (red arrow). (F,G) Dorsal branches showing circumlumenal junctions, formed by type 2 cytokinesis (red arrows). (H) Type 3 cytokinesis showing a new junction that does not run between the daughter nuclei (red arrowhead). (I) Type 3 cytokinesis showing a new junction that forms incorrectly (red arrowhead) and the lateral displacement of the daughter nuclei, in response to ongoing junctional remodeling (orange arrow). (J-M,O) Higher-magnification views showing anti-Dlg staining. (J) Upper cell from D with type 1 junction (red arrowhead). (K) Middle cell from I with type 3 junction (red arrowhead). (L) Upper cell from E with incomplete type 2 cytokinesis (red arrowhead). (M) Middle cell from N with incomplete type 1 cytokinesis (red arrowhead). (N) Type 1 cytokinesis showing an incomplete new junction (red arrowhead) close to the now resorbed autocellular junction. (O) Small anucleated cellular compartment, formed by type 3 cytokinesis, after junctional evolution; borders are indicated by the white bracket. (P) DB after the first round of cell division, with cell borders indicated by the white brackets and showing evolved half-ring junctions (red arrowheads). (Q) Cross-sections (3-µm projections) through a DB that contains an incomplete type 2 circumlumenal junction. (Q′) Sections S1-S5 from Q, showing the position of the nuclei and junctions relative to the lumen. (R) Cross-sections through a DB that contains a type 3 junction. (R′) Sections S1-S5 from R, showing the position of the nuclei and junctions relative to the lumen.

Development (2015) 142, 1794-1805 doi:10.1242/dev.118372

compromise the integrity of the multicellular tube either. For an easier comparison with epithelial cytokinesis (Bourdages and Maddox, 2013), we also include a representation of the tracheal tube as a cylindrical projection (supplementary material Fig. S3A-C), with a duplicated autocellular junction for type 2 and type 3 cytokinesis (supplementary material Fig. S3B,C).

Cell length determines the type of cytokinesis

The number of stalk cells in the DBs usually varies between three and six (Caussinus et al., 2008), and we have found examples of up to seven per branch. Because junctional remodeling and mitosis are parallel processes that take place on a similar time scale, cell division occurs at different time points along the dorsal branches. Both the *de novo* junctions and the new intercellular junctions (formed at the sites of previously autocellular junctions) eventually evolve into similar, alternating half-ring structures. The localization of Myosin II (MyoII) was examined using the Sqh-GFP reporter, and as expected we found accumulations of MyoII at the sites of mitosis (Fig. 3E). We also observed dense accumulations of MyoII (the midbodies) closely associated with the *de novo* junctions that resulted from both type 1 (Fig. 3G) and type 2 (Fig. 3I) cytokinesis. Because the circumlumenal rings produced by type 2 cytokinesis eventually merge with the neighboring intercellular junctions (Fig. 3J), thereby losing their characteristic shape, we had to compromise between recording as many divided cells per branch as possible and being able to distinguish unambiguously between type 1 and type 2 cytokinesis events. Our statistical analysis of cell division included 13 complete DBs that fulfilled these criteria (Fig. 3L,M). Given that the elongation of intercellular junctions is an ongoing and irreversible process, the cells whose nuclei are located above an intercellular junction, or have already entirely abolished their autocellular junction (Fig. 3F) must eventually undergo type 1 cytokinesis. We refer to these cells as possessing 'prospective type 1 junctions'. The converse is true of cells possessing 'prospective type 2 junctions': although at the time of dissection those cells had the potential of undergoing type 2 cytokinesis, given a sufficiently delayed mitosis they may have yet remodeled their junctions sufficiently to undergo type 1 cytokinesis instead. Therefore, the number of cells containing prospective type 2 junctions should be taken as an upper limit. One of the 13 analyzed branches is shown in Fig. 3C-E, together with a color-coded graphical representation (Fig. 3C′-E′) and a summary of the various types of cytokinesis and cell lengths (Fig. 3K). According to our data, on average more than two-thirds of DB stalk cells undergo type 1 cytokinesis, while the remaining ones undergo type 2 cytokinesis. We did not find any examples of type 3 cytokinesis in our sample of 13 DBs, consistent with them being a rare event. The length of the cells is strongly correlated (P<0.001) with the cytokinesis type (Fig. 3M), although the two populations largely overlap, as would be expected if junctional remodeling is not a checkpoint for mitotic entry.

Actomyosin localization during asymmetrical cytokinesis

In dividing cells, the actomyosin cortex is reorganized as part of the well-known process of mitotic rounding (Kunda et al., 2008; Kondo and Hayashi, 2013). Another actin cytoskeleton-based process, the interkinetic nuclear migration (INM), has been observed to re-position nuclei at the apical side in pseudostratified epithelia (Meyer et al., 2011). We observed that during mitosis the nuclei are closely associated with the autocellular junction (Fig. 2R,S1; 2R,S4), whereas the nuclei of pre-mitotic cells and those belonging to non-remodeling branches are located on the opposite side of the tube, relative to the autocellular junction (supplementary material Fig. S2D′). Actin localization during mitosis was explored using the F-actin probe Utrophin-GFP (Herszterg et al., 2013). Compared with the neighboring cells, mitotic cells showed a strong accumulation of actin (Fig. 4A), both at the level of the intercellular junctions (Fig. 4A′,S2) and of the cell cortex (Fig. 4A′,S3,S4). We also observed the accumulation of actin behind the deformed autocellular junction, which is the origin of the *de novo* junction during type 2 cytokinesis (Fig. 4B). In epithelial tissues, the contraction of the actomyosin ring deforms the cell junctions and is the main driving force of cytokinesis (Bourdages and Maddox, 2013). The ingression of the actomyosin ring forms a persistent midbody, close to the site of the emerging junction that eventually separates the two daughter cells (Herszterg et al., 2013). We observed a similar accumulation of MyoII at the site of *de novo* junction formation during type 2 (Fig. 4C) and type 1 (Fig. 4D) cytokinesis.

Timelapse imaging of mitosis in dorsal branches

To better understand the formation of asymmetrical junctions during cytokinesis, we also wanted to acquire movies of the DBs from live specimens. For this purpose, we developed a so-called humid box (see Materials and Methods; supplementary material Fig. S4) and used fast-spinning disk confocal microscopy to reduce the image blurring that is induced by larval movement. Compared with our cold anesthesia method and the recently reported chemical anesthesia setup (Heemskerk et al., 2014), the humid box has several advantages. Most importantly, the larvae can continue to develop during imaging, for up to 12 h. As the lower halves of the larvae are embedded in agarose, only moderate squeezing is sufficient to restrain them, allowing for very high resolution imaging through the transparent cuticle (provided the scanning frequency is above 10-15 Hz). We found that for imaging sessions of less than 30 min, such as for screening purposes, the larvae can also be mounted on glass slides. However, for longer acquisitions, the humid chamber (loaded with a few grams of 7% agarose) was necessary as a source of moisture and as a heat sink. Time points blurred through larval movement were discarded (some 20-50%, depending on the movie) and we used the Volocity software for 3D rendering.

We imaged the transition between a shrinking autocellular junction and a new intercellular junction for several hours in a *E-Cad-GFP;btl-mCherryNLS* larva, at 10 min intervals (Fig. 4E, white arrow). The new multicellular junction formed orthogonal to the old self-junction (Fig. 4E, t=1:20:00) and eventually evolved into a complete half-ring (Fig. 4E, t=2:50:00). Within the same time frame, the upper cell was observed to undergo type 2 cytokinesis (Fig. 4E, red arrow). The mitotic nucleus was closely associated with the autocellular junction and during nuclear envelope breakdown the mCherryNLS was dispersed into the cytoplasm (Fig. 4E, t=0:00:00), revealing the shape of the cell. Autocellular junction deformation and the budding of the *de novo* type 2 junction were also apparent (t=0:20:00 and 0:30:00). Although junctional remodeling continued throughout the duration of the movie (Fig. 4E, orange and white arrows) the type 2 *de-novo* junction failed to extend all the way around the lumen. These results confirm that the extension of the circumlumenal junction can be a protracted affair. Therefore, a large amount of junctional remodeling may take place in the meantime.

We next explored the distribution of MyoII in the DBs of *ubi-H2A-EYFP;Sqh-GFP,E-Cad-tomato* larvae (Fig. 4F). During cytokinesis, the actomyosin ring (t=18:00 to t=21:00, white arrows) was observed to shrink and eventually form a midbody that

Development (2015) 142, 1794-1805 doi:10.1242/dev.118372

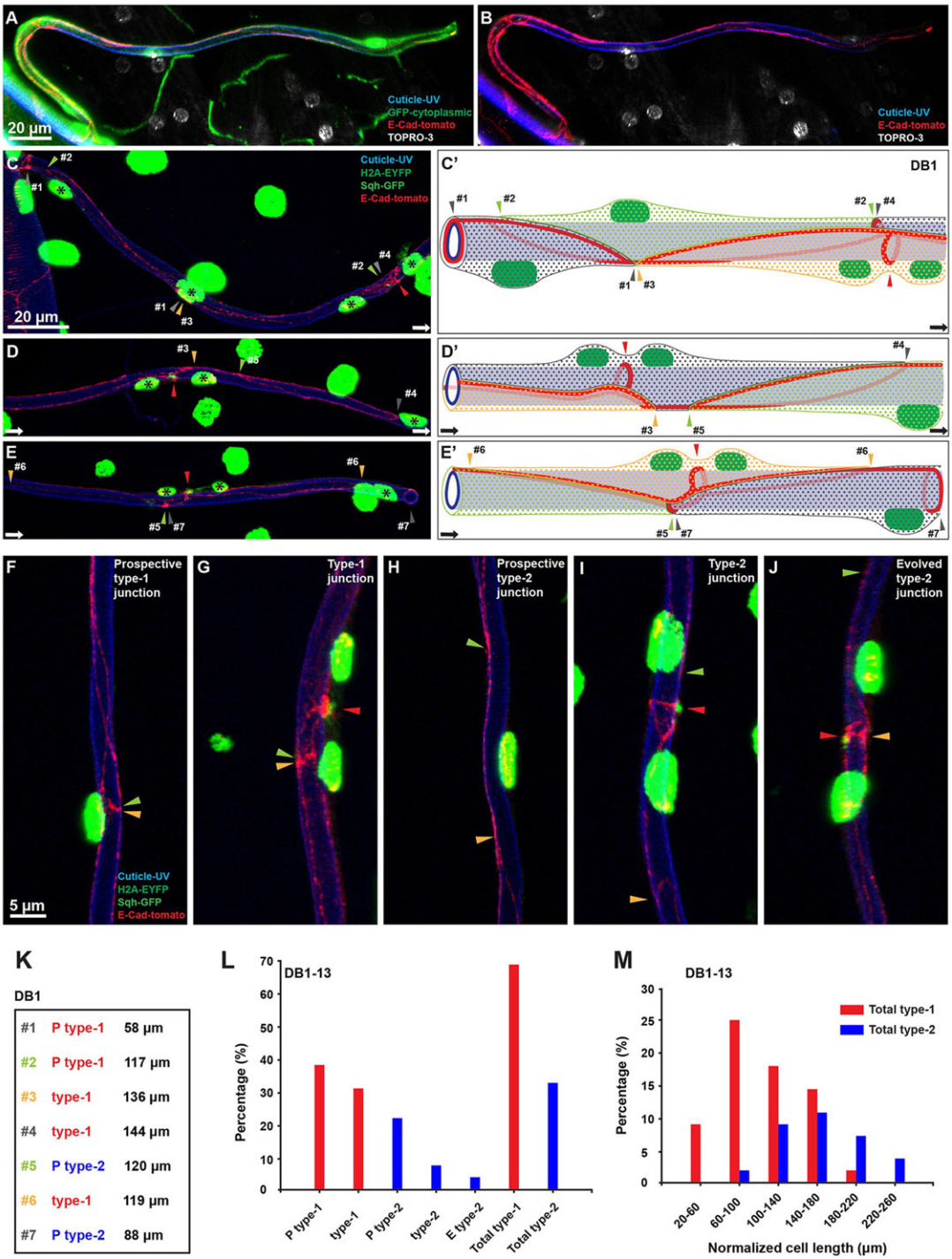

Fig. 3. Dorsal branch architecture and statistics. (A) Dorsal branches from dissected *E-Cad-tomato; btl-Gal4, UAS-GFP* larvae, showing cuticle autofluorescence (blue), stained with anti-GFP/A488 (green), anti-mCherry (red) and TOPRO-3 (white). (B) The branch from A without showing cytoplasmic GFP. (C-E) Complete dorsal branch from a dissected *H2A-EYFP*; *E-Cad-tomato; Sqh-GFP* larva, showing cuticle autofluorescence (blue), stained with anti-GFP/A488 (green) and anti-mCherry (red). Nuclei belonging to the DB are highlighted by a black asterisk, the new junctions are indicated by red arrowheads, the borders of the seven cells are indicated by color-coded arrowheads and the white arrows show the order of the cells along the DB. (C′-E′) Graphic representation of the dorsal branch from C-E, using the same color code to indicate the seven stalk cells. (F-J) Examples of cells that have undergone, or are about to undergo, type 1 or type 2 cytokinesis. (F) DB cell that has completely resorbed the autocellular junction (at the position of the green and orange arrowheads) and therefore must eventually undergo type 1 cytokinesis. (G) New junction formed by type 1 cytokinesis (red arrowhead) close to the intercellular junction (green and orange arrowheads). (H) DB cell that retains the autocellular junction (shown between the green and orange arrowheads) and may undergo type 2 cytokinesis. (I) New circumlumenal junction formed by type 2 cytokinesis (red arrowhead) from an autocellular junction (shown between the green and orange arrowheads). (J) Evolved type 2 junction (red arrowhead) showing an intercellular junction that made contact with the lower side of the circumlumenal junction (orange arrowhead), while the upper part remains autocellular (green arrowhead). (K) Cell size and the types of cytokinesis observed in the DB from C-E. (L) Percentages of the type 1 and type 2 cytokinesis from six larvae, 13 DBs (Tr3 or Tr4), n=56 cells. (M) Normalized distribution of type 1 (n=28) and type 2 DB cells (n=18) according to their length. The two cell populations are statistically distinct (P<0.001).

Development (2015) 142, 1794-1805 doi:10.1242/dev.118372

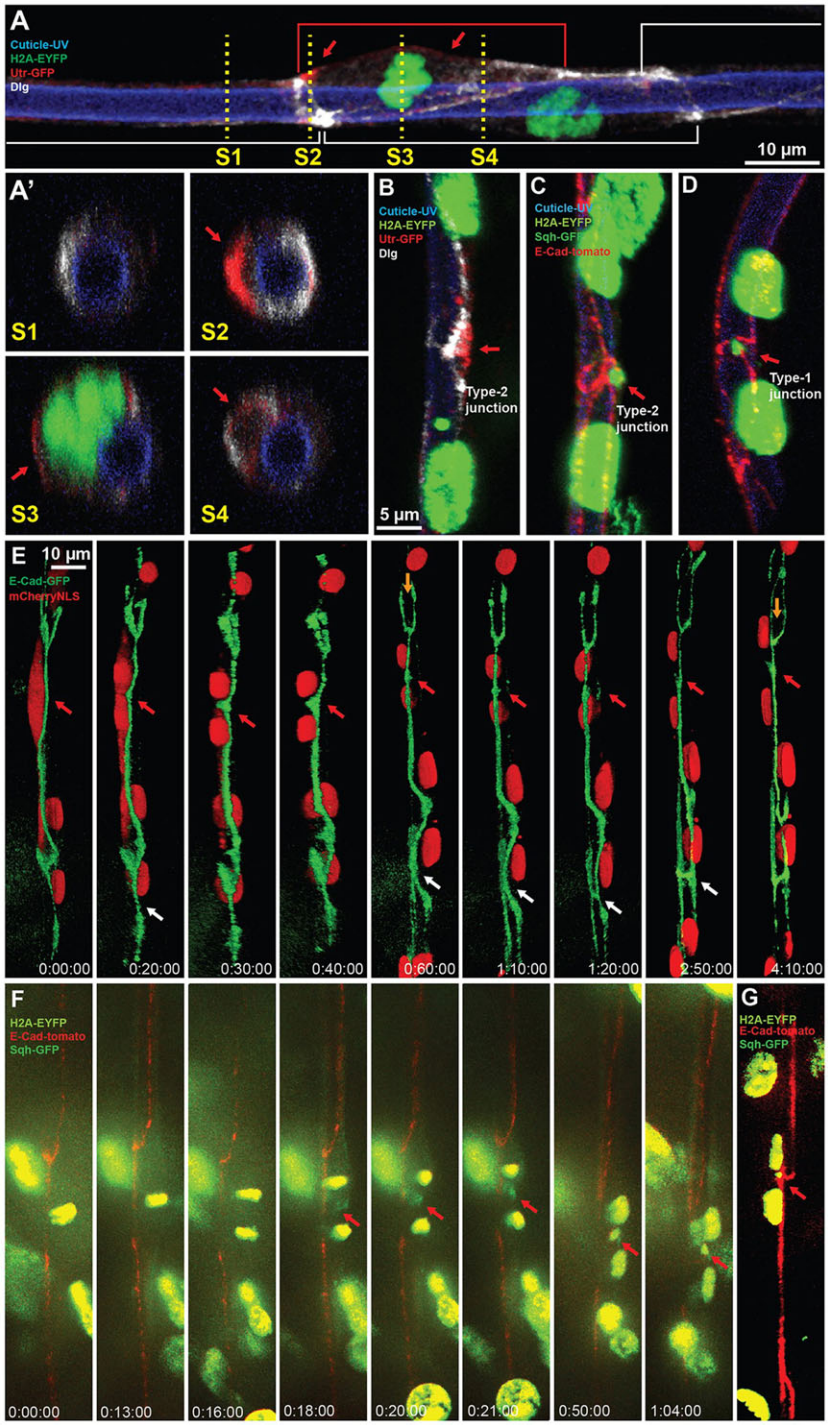

Fig. 4. Actomyosin and time lapse imaging. (A,B) DBs from dissected *H2A-EYFP*, *Utr-GFP* larva, showing cuticle autofluorescence (blue) and stained with anti-GFP/A488 (red) and anti-Dlg (white). (A) The red bracket marks the mitotic cell, the white brackets indicate the neighboring cells and the red arrows indicate the accumulation of actin at the cell cortex and at the intercellular junction. (A′) Cross-sections through the DB from D. S1 shows low levels of actin in the leftmost cell. S2 shows high levels of actin at the level of the intercellular junction of the mitotic cell. S3 shows the actin cortex at the level of the metaphase plate. S4 shows comparatively higher levels of actin accumulation in the cortex of the rounded mitotic cell, compared with its counterpart on the other side of the DB. (B) Incomplete type 2 cytokinesis showing actin accumulation behind the vertex of a deformed autocellular junction (red arrow). (C,D) DBs from dissected *H2A-EYFP*; *E-Cad-tomato; Sqh-GFP* larvae, showing cuticle autofluorescence (blue), stained with anti-GFP/A488 (green) and anti-mCherry (red). (C) Completed type 2 cytokinesis, the position of the midbody is indicated by a red arrowhead. (D) Type 1 cytokinesis showing junctional deformation and the position of the midbody (red arrow). (E-G) Snapshots from movies acquired with the humid box at the spinning disk confocal. (E) Tr3 DB, *E-Cad-GFP* (green) and *btl-mCherryNLS* (red) showing incomplete type 2 cytokinesis (red arrows) (supplementary material Movie 1). Shrinkage of an autocellular junction and formation of a new transverse intercellular junction, as per type 1 cytokinesis (white arrows). Extension of intercellular junction towards the new junction (orange arrow). (F) Tr4 DB, *ubi-H2A-EYFP* (yellow), Sqh-GFP (green) and E-Cad-*tomato* (red) showing actomyosin ring and midbody formation (red arrows) (supplementary material Movie 2). (G) Tr3 DB, *ubi-H2A-EYFP* (yellow), Sqh-GFP (green) and E-Cad-*tomato* (red) showing the deformation of the autocellular junction adjacent to the midbody and a partial circumlumenal ring (red arrow).

Development (2015) 142, 1794-1805 doi:10.1242/dev.118372

remained closely associated with the autocellular junction (Fig. 4F, t=1:04:00). The midbody came to reside at the apical side of the cell (close to the lumen of the tube), similar to what was observed in other epithelial tissues (Founounou et al., 2013; Guillot and Lecuit, 2013; Herszterg et al., 2013). Furthermore, the midbody was located close to the tip of the deformed autocellular junction, as we observed in a separate short movie (Fig. 4G). The *de novo* junction emerged as an extension from the vertex of the furrowed autocellular junction (Fig. 4G), in agreement with our data from immunostaining (Fig. 4C,D).

The Dpp pathway is activated in all the tracheal branches that undergo remodeling

Tracheal remodeling is a coordinated process that takes place in only a subset of branches: the contrast between the remodeling seen in the DB of Tr5, and the lack thereof in the DB of Tr6, is particularly striking. We investigated the activity of the Dpp pathway, a known regulator of DB fate in the embryo (Ribeiro et al., 2004), in staged larvae using *dad-GFP* and *brk-Gal4,UAS-mCherry* as reporters. High levels of Dad and low levels of Brk result from increased Dpp signaling, and *dad-GFP* was shown to be an effective Dpp signaling readout (Ninov et al., 2010; Weiss et al., 2010). By 3 h into L3, the Dpp pathway was found to be activated within the spiracular branches of all tracheomeres (supplementary material Fig. S5A,D), as well as in the dorsal branches of Tr2-Tr5 (supplementary material Fig. S5A-C). The first cell divisions in the DB and DT of Tr2 take place about 18 h into L3 and Dpp signaling was detectable several hours before the event (supplementary material Fig. S5E). We observed a wave of Dpp activity from anterior to posterior that preceded and was strongly correlated with the remodeling of tracheal system throughout the third instar (Fig. 5L-N). Low levels of Dpp signaling were seen in the non-remodeling DBs and DTs of abdominal tracheomeres (Tr6-Tr10) towards the end of the third instar (supplementary material Fig. S5P).

To analyze the possible role of Dpp signaling in the remodeling of dorsal branches, we overexpressed either the pathway repressor Dad (*UAS-dad*) or the constitutively active receptor (*UAS-Tkv^{QD}*) under the control of *btl-Gal4*. As DB formation in the embryo requires Dpp signaling (Ribeiro et al., 2004), we used *tub::Gal80^{ts}* for temporal control of the *UAS* transgenes. The animals were grown at 18°C for 2 days and then allowed to continue development at 29°C until the WL stage. During L3, the activity of the *btl* promoter is known to be relatively low outside of the remodeling DBs and SBs (Weaver and Krasnow, 2008), so we used a *tub>CD2>Gal4* cassette under *btl-Gal4*,*UAS-Flp* control to maintain high levels of Gal4 in all the tracheal cells (Fig. 5A-F,S-U). Depending on the larval genotype (*tub>CD2>Gal4,UAS-lacZ* or *CyO,wg-lacZ*), β-Gal was present in the nuclei of the tracheal cells (Fig. 5A-F,S-U) or in the *wg* domain of the wing disk (data not shown). Dad overexpression, driven by the combined *btl* and *tub* promoters, resulted in a two- to threefold reduction in the number of cells in the Tr2-Tr4 DB (Fig. 5A-D), as well as a mosaic pattern of large and small nuclei that is not seen in the controls (Fig. 5D, yellow arrow). We observed a similar effect, albeit of lower magnitude, when Dad was overexpressed under the control of the *btl* promoter alone (Fig. 5I-K). The remodeling of the DB from Tr2 was found to be less sensitive to Dad overexpression, compared with the DBs of Tr3-Tr5 (Fig. 5A). The DBs of *dad-GFP* (Fig. 5L-N) and *btl-mCherry* (Fig. 5O-R) larvae are shown as controls. We also investigated the link between Dpp downregulation and junctional remodeling during the mid-L3 stage (Fig. 5E-H). The characteristic elongation of the intercellular junctions was severely delayed by the presence of high levels of ectopic Dad (compare Fig. 5E,F with Fig. 1C). Low levels of Dad overexpression had little impact on the timing of junctional remodeling (Fig. 5G,H), consistent with the results from WL stage (Fig. 5I-K).

Conversely, ectopic expression of Tkv^{QD} did not induce cell proliferation in the anterior DBs beyond the limits of that particular niche, as opposed to the dramatic proliferation that can be induced by PI3K overexpression (data not shown). Both the high (Fig. 5S-U) and the low (Fig. 5V-X) levels of induction resulted in similar outcomes. Importantly, the overexpression of Tkv^{QD} did not induce proliferation in the abdominal Tr6-Tr10 DBs either (data not shown). Therefore, we conclude that Dpp signaling is necessary but not sufficient for remodeling in the DBs.

DISCUSSION

The adult tracheal system of *Drosophila* comprises regions that have been carried over from the larval stage, as well as new structures that originated from pools of imaginal cells. The precursor cells that will go on to form the air sacs (Sato and Kornberg, 2002), the spiracles (Pitsouli and Perrimon, 2010), the abdominal trachea (Chen and Krasnow, 2014) and the coiled tracheolar cells (Weaver and Krasnow, 2008) retain their proliferative potential until the third instar, when they begin to undergo multiple rounds of division. During the pupal stage, they divide, migrate and differentiate, thereby replacing histolyzed tissues such as the abdominal tracheomeres (Chen and Krasnow, 2014) and forming new structures, such as the air sacs. Alone among tracheal metameres, remodeling in Tr2 also includes the DT and VB. The special identity of Tr2, where the ASP originates (Sato and Kornberg, 2002), is specified by a Hox code (Sato et al., 2008; Djabrayan et al., 2014). It is interesting that the cells in the DB of Tr2 divide a few hours earlier than those from the other anterior tracheomeres and generally have thicker branches by the WL stage (Fig. 5O-R).

Proliferation in the dorsal branch is preceded by junctional rearrangement

As previous studies have shown, the cells in the DBs of Tr2-Tr5 will continuously divide throughout the third instar (Sato et al., 2008; Weaver and Krasnow, 2008). The embryonic transition from a multicellular tube to a unicellular tube with autocellular junctions takes place in the absence of cell division (Ribeiro et al., 2004; Neumann and Affolter, 2006) and is an extreme example of tubular epithelial morphogenesis. We sought a new model system that would incorporate cell division as part of the developmental process. To this end, we investigated the larval dorsal branches at the cellular level, with the aid of high-resolution images from dissected larvae and live imaging methods that we have developed specifically for this task.

We found that, prior to mitosis, the characteristic autocellular junctions of the DBs undergo remodeling, likely driven by changes in actomyosin force distribution, as has previously been shown to be the case in epithelial tissues (Lecuit, 2005). The intercalation process is not a prerequisite condition for the formation of the *de novo* junctions, as cytokinesis can take place in cells that retain part of their self-junctions (Fig. 2G). Mitotic cell rounding within an epithelium has been shown to be a key process in the invagination of the *Drosophila* tracheal placode (Kondo and Hayashi, 2013), and the mitotic rounding of the DB cells (Fig. 4A) is likely the driving force behind the changes in cell shape, as well as the associated elongation of the intercellular junctions at the expense of the autocellular ones. As we have shown, cell division in the DBs is highly directional along the lumen (Fig. 3C-E). During cytokinesis, the membrane furrows on the side of the cell where the nucleus

Development (2015) 142, 1794-1805 doi:10.1242/dev.118372

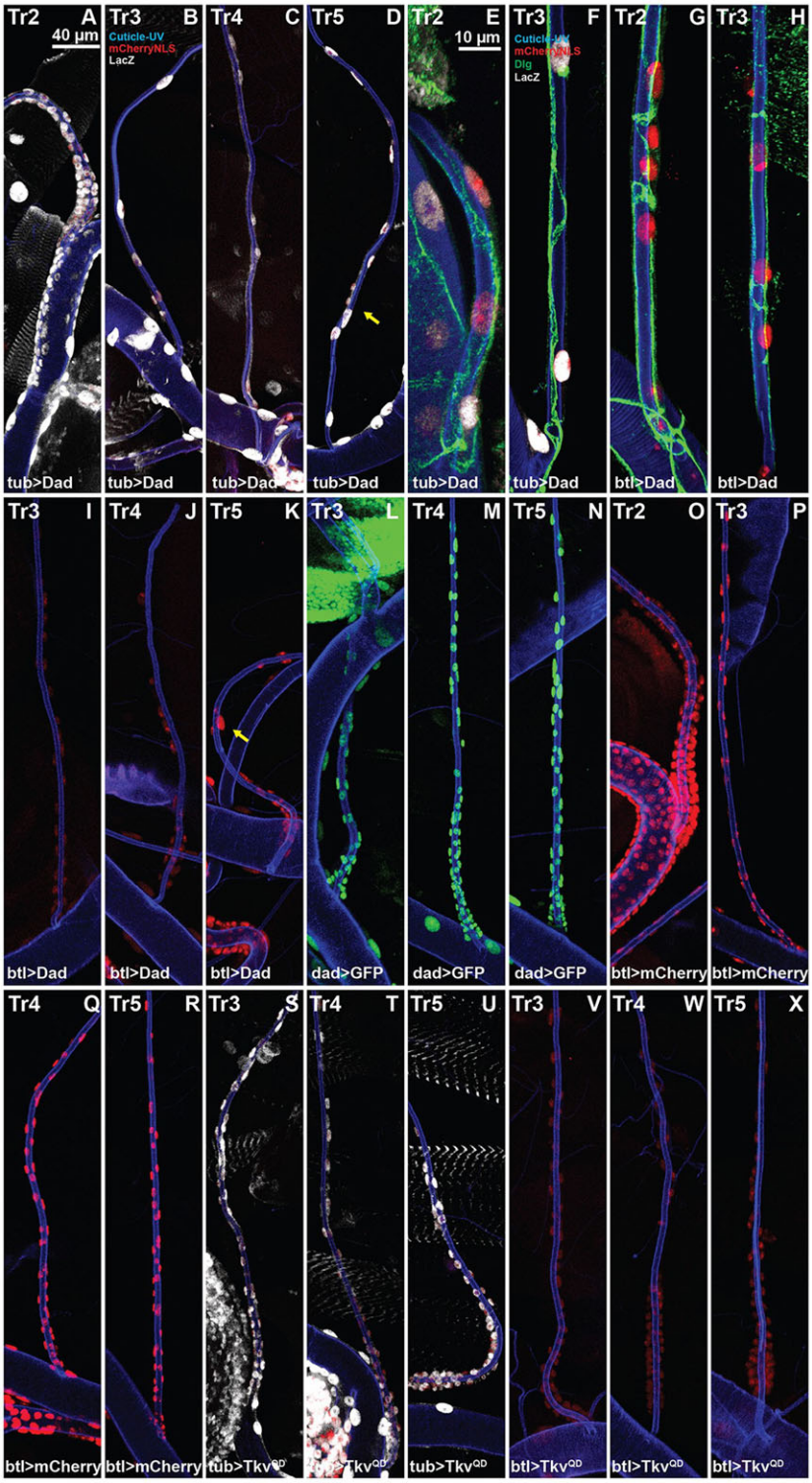

Fig. 5. Lower levels of Dpp translate into less remodeling in the dorsal branches. (A-D) High levels of Dad overexpression, driven by btl-Gal4 together with tub-Gal4 (*n*=5, Tr2-Tr6), greatly reduce the number of cells in the DBs of the WL stage; btl-mCherryNLS (red), lumen autofluorescence (blue) and anti-β-Gal (white). (D) Adjacent large and small nuclei (yellow arrow). (E,F) High levels of Dad overexpression result in delayed junctional remodeling in mid-L3 larvae (*n*=4, Tr2-Tr6); btl-mCherryNLS (red), anti-Dlg (green), lumen autofluorescence (blue) and anti-β-Gal (white). (G,H) Intermediate levels of Dad overexpression, driven by btl-Gal4, allow normal junctional remodeling in mid-L3 larvae (*n*=4, Tr2-Tr6); btl-mCherryNLS (red), anti-Dlg (green) and lumen autofluorescence (blue). (I-K) Intermediate levels of Dad overexpression, driven by btl-Gal4, reduce number of cells in the DBs of the WL stage (*n*=5, Tr2-Tr6); btl-mCherryNLS (red) and lumen autofluorescence (blue). (K) Adjacent large and small nuclei (yellow arrow). (L-N) Dpp activity in the DBs of control WL stage (*n*=5, Tr2-Tr6), as shown by the dad-GFP reporter. (O-R) DBs from control WL stage (*n*=5, Tr2-Tr6), showing wild-type levels of dorsal branch remodeling; btl-mCherryNLS (red), lumen autofluorescence (blue). (S-U) High levels of Tkv^{QD} overexpression (*n*=5, Tr2-Tr6), driven by btl-Gal4 and tub-Gal4, do not greatly increase cell numbers in the dorsal branch; btl-mCherryNLS (red), lumen autofluorescence (blue) and anti-β-Gal (white). (V-X) Intermediate levels of Tkv^{QD} overexpression, driven by btl-Gal4 (*n*=5, Tr2-Tr6), also do not affect cell numbers; btl-mCherryNLS (red) and lumen autofluorescence (blue).

Development (2015) 142, 1794-1805 doi:10.1242/dev.118372

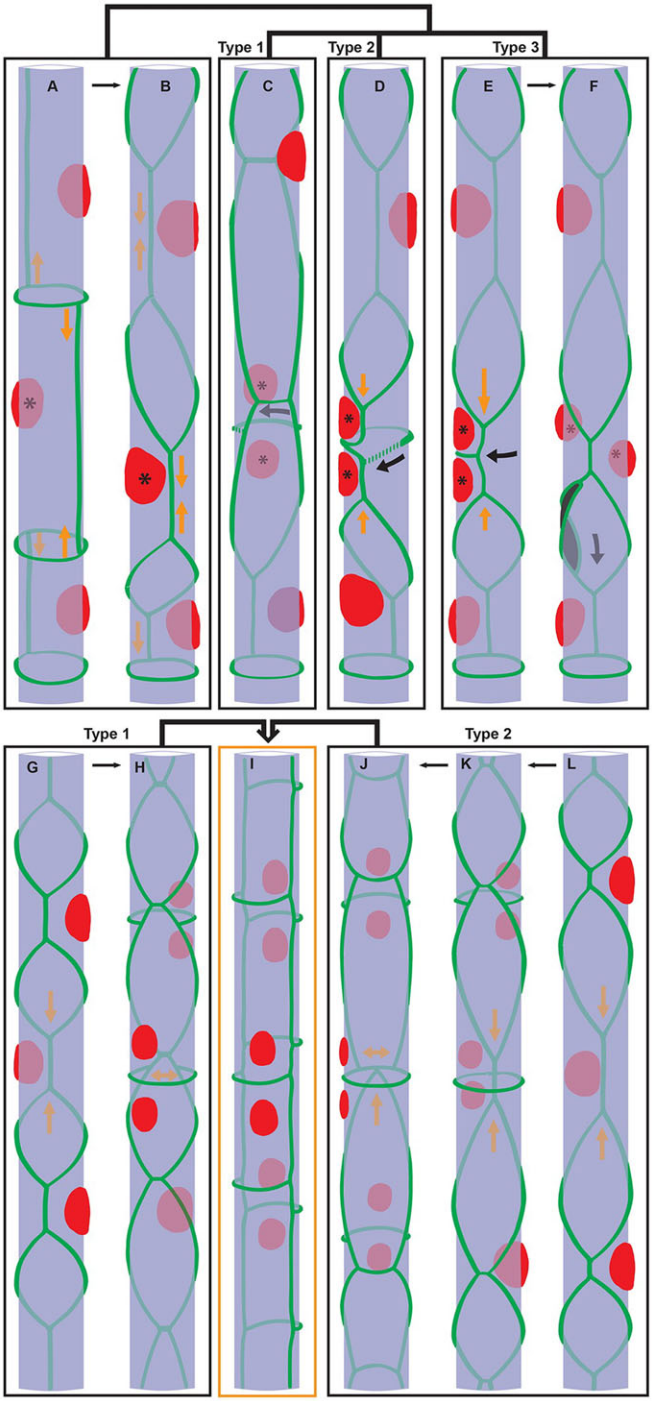

Fig. 6. 3D model of dorsal branch remodeling. (A) Dorsal branch in early L3 before remodeling, showing the cellular junctions (green), the nuclei (red) and the lumen (blue). The intercellular junctions elongate at the expense of the autocellular junctions, as shown by the orange arrows. (B) Expanded intercellular junctions and shortened autocellular junctions. (C) Type 1 cytokinesis, with half ring formation in a multicellular tube (arrow). (D) Type 2 cytokinesis with circumlumenal ring initiation at the apex of the deformed autocellular junction, separating the daughter cells before the tube has become multicellular (black arrow). (E) Type 3 cytokinesis showing different rates of elongation in the flanking intercellular junctions (orange arrows) and slow progression of the circumlumenal ring (black arrow). (F) Type 3 cytokinesis with displaced nuclei and displaced junction (arrow); the daughters are a bi-nucleated cell and an anucleated cell (dark gray). (G) Closely packed cells undergoing junctional remodeling (orange arrows). (H) Type 1 remodeling, showing the transition to a multicellular tube prior to cell division. The new intercellular junctions that form at the spot of the former autocellular junctions extend around the lumen (orange double arrow). (I) Alternating ladder structure that is the convergent outcome of both type 1 and type 2 remodeling. (J) The circumlumenal ring makes contact with the neighboring intercellular junctions and is eventually split in two half-rings (orange arrows) that come to occupy positions in trans. (K) Type 2 cytokinesis in a unicellular tube. (L) Well-spaced cells undergoing junctional remodeling (orange arrows).

is located (Fig. 4E) and the new junction extends around the lumen until it connects with another membrane (Fig. 4C,D). The actomyosin rings that drive cytokinesis in the *Drosophila* epithelia are able to symmetrically deform the AJs of the two cells that flank the emerging junction (Founounou et al., 2013; Guillot and Lecuit, 2013; Herszterg et al., 2013). We find that in the remodeling dorsal tracheal branches, asymmetric *de novo* junction formation is the norm: presumably, the peculiar geometry of the unicellular tubes favors this outcome. The unicellular tubes that undergo type 2 cytokinesis do not have neighboring cells close to the plane of division that might assist the membrane furrowing process, as in epithelial sheets (Herszterg et al., 2013). Those differences notwithstanding, the actin accumulation behind the deformed autocellular junction (Fig. 4B) and the position of the midbody near the tip of the *de novo* junction (Fig. 4C,D) bears an uncanny resemblance to the mitotic machinery described in epithelial cells (Bourdages and Maddox, 2013). As all the DB cells are potentially capable of dividing in this fashion, we documented the various ways of completing cytokinesis, as summarized in Fig. 6. According to our results, the intercellular junctions continue to remodel in parallel with cytokinesis (Fig. 6C,D). It follows that there are multiple ways in which cytokinesis may be completed, depending on the position of the intercellular junctions relative to the autocellular junctions (Fig. 6C-F). Our analysis has identified three possible outcomes. In type 1 cytokinesis, the emerging junction intersects with an intercellular junction (supplementary material Fig. S3,A5 and Fig. 6C). In the case of type 2 cytokinesis, the junction connects to the other side of the autocellular junction (supplementary material Fig. S3,B5 and Fig. 6D) and forms a circumlumenal ring (Fig. 2G). Finally, in type 3 cytokinesis, the nuclei are pushed away from the growing junction by the ongoing remodeling process (supplementary material Fig. S3,C3) and the asymmetric junction that normally runs between the daughter nuclei, intersecting with the membrane on the opposite side of the cell, fuses to the proximal side of the cell instead (supplementary material Fig. S3,C5 and Fig. 6F). Through this unequal division the cell is partitioned into a bi-nucleated and an anucleated daughter cell (Fig. 6F).

This apparent lack of specificity does not result in an uncoordinated development. We find that the daughter cells that are the outcome of type 1 (Fig. 6G,H) and type 2 (Fig. 6J-L) cytokinesis continue to undergo junctional evolution (Fig. 2P), ultimately producing a distinct, alternating ladder architecture (Fig. 6I). In conclusion, the remodeling of the dorsal branches has at its core a dramatic junctional rearrangement and a robust mechanism of asymmetric cytokinesis.

Dorsal branch remodeling requires Dpp signaling

We have found that Dpp signaling is activated in all the tracheal regions that undergo remodeling in the third instar, namely the SBs, the anterior DBs and the DT of Tr2 (supplementary material Fig. S5). Low levels of activation were seen in the non-remodeling tracheal branches (supplementary material Fig. S5O,P). Dad overexpression (Fig. 5A-D) reduced the number of cells in the DBs by approximately a factor of three, compared with the controls

Development (2015) 142, 1794-1805 doi:10.1242/dev.118372

(Fig. 5L-R). The downregulation of Dpp signaling delays both junctional remodeling and mitosis (Fig. 5E,F), so Dpp is likely required as a permissive factor for cell cycle re-entry in the DB cells. Within the abdominal DBs of late L3 wild-type larvae, medium levels of Dpp signaling do not lead to remodeling (supplementary material Fig. S5P). This is consistent with our inability to induce remodeling ectopically by overexpressing the constitutively active receptor Tkv^{QD} in those segments. Therefore, in addition to its role in the formation of the embryonic DBs, Dpp signaling is also involved in the later development of the larval trachea, presumably in conjunction with other, so far unidentified, factors.

MATERIALS AND METHODS

Fly stocks

We used the fly stocks *E-Cad-GFP*, *E-Cad-tomato*, *E-Cad-GFP;btl-mCherryNLS*, *ubi-H2A-EYFP;Sqh-GFP,E-Cad-tomato*, *ubi-H2A-EYFP; Utr-GFP,Sqh-mCherry/CyO*, *Brk-Gal4;UAS-mCherryNLS;dad4-EGFPnls*, *UAS-mCherryNLS*, *UAS-Tkv^{QD}*, *UAS-dad, tub-Gal80^{ts}, hs-Flp*, *UAS-Flp, btl-mCherryNLS*, *UAS-dad,UAS-Flp;btl-Gal4,tub-Gal80^{ts}*, *tub-Gal80^{ts};UAS-Flp,act-Gal4*, *UAS-Flp;btl-Gal4,tub-Gal80^{ts}*, *tub-FRT>CD2>FRT-Gal4*, *UAS-lacZ/CyO,wg-LacZ;btl-mCherryNLS*, *tub-FRT>CD2>FRT-Gal4,UAS-lacZ/CyO,wg-LacZ;UAS-Tkv^{QD},btl-mCherryNLS* and *Raeppli.NLS53D,89A*.

Larval staging

Flies were flipped on fresh food every day and maintained at 25°C for 5 days; for the $Gal80^{ts}$ experiments they were incubated at 18°C for 8 days. The late L2 stage larvae were collected (based on the morphology of the anterior spiracles) and allowed to hatch on agar plates. After 3 h, the freshly hatched L3 larvae were transferred to fresh food vials and incubated at 25 or 29°C until the desired age.

Immunohistochemistry

For dissection, the anesthetized larvae (up to 1 h incubation on ice) were transferred in a drop of chilled PBS on a silicone plate, immobilized with needles and opened on the ventral side. After removing everything apart from the tracheal system and the associated imaginal disks, the carcasses were fixed in 1% PFA for 15 min, washed with PBT (1× PBS buffer with 0.3% Triton X-100) and transferred to 24-well plates. We used the following antibodies: mouse anti-Dlg (1:1000, Hybridoma Bank), rabbit anti-GFP (1:2000; Abcam, ab6556), rabbit anti-β-Gal (1:5000; Cappel, 55976) and rabbit anti-mCherry (1:10,000, a gift from the Erich Nigg lab, University of Basel, Switzerland). Anti-mouse and anti-rabbit secondary antibodies, conjugated to Alexa Fluor 488, 568 and 633 were used at a dilution of 1:1000.

Imaging

Fixed samples were imaged with a Leica SP5 point scanning confocal. Data processing was carried out with Imaris, including the distance measurements using the Point function. Statistical significance was assessed by the Kolmogorov–Smirnov test. Following our observation that *Drosophila* larvae can survive being cooled to sub-zero temperatures, we constructed a special device in collaboration with the Mechanical and Electronic Workshops at the Biozentrum (Basel, Switzerland) (supplementary material Fig. S1). The device uses a Peltier element to cool an aluminium plate to a temperature of approximately −3°C. The heat from the warm side is dissipated by means of a radiator and a side fan. The plate is shaped to fit on the microscope table and can accommodate a glass slide. The larva was mounted on a slide, using adhesive tape and capillarity to achieve the right amount of pressure (supplementary material Fig. S1D). Two paper stripes were used to protect the larva from glycerol immersion, while a bit of 2% methylcellulose was applied to the coverslip in order to prevent droplet condensation above the sample. Owing to the high thermal conductivity of immersion objectives, a 20× air objective was used for all the experiments. After data acquisition, the larvae were transferred to grape juice plates supplemented with fly food and allowed to continue development in a humidified box, at the appropriate temperature.

Time-lapse imaging was performed with a humid chamber, also constructed by the Mechanical Workshop (supplementary material Fig. S4). A special slide was prepared for each experiment, by casting 7% agarose in a plexiglas mold (supplementary material Fig. S4D). The agarose was trimmed level with the surface using a blade, the tape spacers were added and the larva was mounted on the central patch. After adding the coverslip, the larva was allowed to settle for half an hour into the agarose and then the whole slide was lowered inside the humid chamber. Glycerol was used to seal the interface between the slide and the bottom of the chamber. As the humid chamber does not cool the larvae, we used a fast scanning mode to minimize blurring from the gut peristalsis. Movies were acquired on a PerkinElmer Ultraview spinning disk confocal with a 63× immersion objective, at a frame rate of 15 Hz. Image processing was carried out using the Volocity software and Fiji.

Acknowledgements

We thank the Mechanical and the Electronic Workshops at the Biozentrum for building our custom devices; the Imaging Core Facility for help with confocal microscopy; and Y. Bellaiche, E. Caussinus, F. Hamaratoglu, M. Müller and A. Ochoa-Espinosa for flies and ideas.

Competing interests

The authors declare no competing or financial interests.

Author contributions

A.S.D. designed the two imaging methods, acquired the data and constructed the model. A.S.D. devised and conducted the Raeppli experiments for Fig. 1E and the Dpp experiments in Fig. 5 with the help of O.K. A.S.D. and M.A. wrote the manuscript.

Funding

This work was supported by grants from the Swiss National Science Foundation and from Cantons BS and BL. A.S.D. was partly supported by an EMBO fellowship. O.K. was funded by the SystemsX.ch initiative.

Supplementary material

Supplementary material available online at
http://dev.biologists.org/lookup/suppl/doi:10.1242/dev.118372/-/DC1

References

Affolter, M. and Caussinus, E. (2008). Tracheal branching morphogenesis in Drosophila: new insights into cell behaviour and organ architecture. *Development* **135**, 2055-2064.

Blanpain, C. and Fuchs, E. (2009). Epidermal homeostasis: a balancing act of stem cells in the skin. *Nat. Rev. Mol. Cell Biol.* **10**, 207-217.

Bourdages, K. G. and Maddox, A. S. (2013). Dividing in epithelia: cells let loose during cytokinesis. *Dev. Cell* **24**, 336-338.

Caussinus, E., Colombelli, J. and Affolter, M. (2008). Tip-cell migration controls stalk-cell intercalation during Drosophila tracheal tube elongation. *Curr. Biol.* **18**, 1727-1734.

Chen, F. and Krasnow, M. A. (2014). Progenitor outgrowth from the niche in Drosophila trachea is guided by FGF from decaying branches. *Science* **343**, 186-189.

Chen, C. K., Kuhnlein, R. P., Eulenberg, K. G., Vincent, S., Affolter, M. and Schuh, R. (1998). The transcription factors KNIRPS and KNIRPS RELATED control cell migration and branch morphogenesis during Drosophila tracheal development. *Development* **125**, 4959-4968.

Djabrayan, N. J.-V., Cruz, J., de Miguel, C., Franch-Marro, X. and Casanova, J. (2014). Specification of differentiated adult progenitors via inhibition of endocycle entry in the Drosophila trachea. *Cell Rep.* **9**, 859-865.

Edgar, B. A. and Orr-Weaver, T. L. (2001). Endoreplication cell cycles: more for less. *Cell* **105**, 297-306.

Founounou, N., Loyer, N. and Le Borgne, R. (2013). Septins regulate the contractility of the actomyosin ring to enable adherens junction remodeling during cytokinesis of epithelial cells. *Dev. Cell* **24**, 242-255.

Fox, D. T., Gall, J. G. and Spradling, A. C. (2010). Error-prone polyploid mitosis during normal Drosophila development. *Genes Dev.* **24**, 2294-2302.

Ghabrial, A., Luschnig, S., Metzstein, M. M. and Krasnow, M. A. (2003). Branching morphogenesis of the Drosophila tracheal system. *Annu. Rev. Cell Dev. Biol.* **19**, 623-647.

Giangreco, A., Arwert, E. N., Rosewell, I. R., Snyder, J., Watt, F. M. and Stripp, B. R. (2009). Stem cells are dispensable for lung homeostasis but restore airways after injury. *Proc. Natl. Acad. Sci. USA* **106**, 9286-9291.

Guha, A. and Kornberg, T. B. (2005). Tracheal branch repopulation precedes induction of the Drosophila dorsal air sac primordium. *Dev. Biol.* **287**, 192-200.

Development (2015) 142, 1794-1805 doi:10.1242/dev.118372

Guha, A., Lin, L. and Kornberg, T. B. (2008). Organ renewal and cell divisions by differentiated cells in Drosophila. *Proc. Natl. Acad. Sci. USA* **105**, 10832-10836.
Guillot, C. and Lecuit, T. (2013). Adhesion disengagement uncouples intrinsic and extrinsic forces to drive cytokinesis in epithelial tissues. *Dev. Cell* **24**, 227-241.
Harris, T. J. C. and Tepass, U. (2010). Adherens junctions: from molecules to morphogenesis. *Nat. Rev. Mol. Cell Biol.* **11**, 502-514.
Heemskerk, I., Lecuit, T. and LeGoff, L. (2014). Dynamic clonal analysis based on chronic in vivo imaging allows multiscale quantification of growth in the Drosophila wing disc. *Development* **141**, 2339-2348.
Herszterg, S., Leibfried, A., Bosveld, F., Martin, C. and Bellaiche, Y. (2013). Interplay between the dividing cell and its neighbors regulates adherens junction formation during cytokinesis in epithelial tissue. *Dev. Cell* **24**, 256-270.
Huang, J., Zhou, W., Dong, W., Watson, A. M. and Hong, Y. (2009). Directed, efficient, and versatile modifications of the Drosophila genome by genomic engineering. *Proc. Natl. Acad. Sci. USA* **106**, 8284-8289.
Kanca, O., Caussinus, E., Denes, A. S., Percival-Smith, A. and Affolter, M. (2014). Raeppli: a whole-tissue labeling tool for live imaging of Drosophila development. *Development* **141**, 472-480.
Kondo, T. and Hayashi, S. (2013). Mitotic cell rounding accelerates epithelial invagination. *Nature* **494**, 125-129.
Kunda, P., Pelling, A. E., Liu, T. and Baum, B. (2008). Moesin controls cortical rigidity, cell rounding, and spindle morphogenesis during mitosis. *Curr. Biol.* **18**, 91-101.
Lecuit, T. (2005). Adhesion remodeling underlying tissue morphogenesis. *Trends Cell Biol.* **15**, 34-42.
Manning, G. and Krasnow, M. A. (1993). Development of the Drosophila tracheal system. In *The Development of Drosophila melanogaster* (ed. M. Bate and A. Martinez-Arias), pp. 609-685. Woodbury, NY: Cold Spring Harbor Laboratory Press.
Martin, P. and Parkhurst, S. M. (2004). Parallels between tissue repair and embryo morphogenesis. *Development* **131**, 3021-3034.
Maruyama, R. and Andrew, D. J. (2012). Drosophila as a model for epithelial tube formation. *Dev. Dyn.* **241**, 119-135.
Meyer, E. J., Ikmi, A. and Gibson, M. C. (2011). Interkinetic nuclear migration is a broadly conserved feature of cell division in pseudostratified epithelia. *Curr. Biol.* **21**, 485-491.
Neumann, M. and Affolter, M. (2006). Remodelling epithelial tubes through cell rearrangements: from cells to molecules. *EMBO Rep.* **7**, 36-40.
Ninov, N., Menezes-Cabral, S., Prat-Rojo, C., Manjon, C., Weiss, A., Pyrowolakis, G., Affolter, M. and Martin-Blanco, E. (2010). Dpp signaling directs cell motility and invasiveness during epithelial morphogenesis. *Curr. Biol.* **20**, 513-520.
Pitsouli, C. and Perrimon, N. (2010). Embryonic multipotent progenitors remodel the Drosophila airways during metamorphosis. *Development* **137**, 3615-3624.
Ribeiro, C., Ebner, A. and Affolter, M. (2002). In vivo imaging reveals different cellular functions for FGF and Dpp signaling in tracheal branching morphogenesis. *Dev. Cell* **2**, 677-683.
Ribeiro, C., Neumann, M. and Affolter, M. (2004). Genetic control of cell intercalation during tracheal morphogenesis in Drosophila. *Curr. Biol.* **14**, 2197-2207.
Rock, J. R. and Hogan, B. L. M. (2011). Epithelial progenitor cells in lung development, maintenance, repair, and disease. *Annu. Rev. Cell Dev. Biol.* **27**, 493-512.
Samakovlis, C., Hacohen, N., Manning, G., Sutherland, D. C., Guillemin, K. and Krasnow, M. A. (1996). Development of the Drosophila tracheal system occurs by a series of morphologically distinct but genetically coupled branching events. *Development* **122**, 1395-1407.
Sato, M. and Kornberg, T. B. (2002). FGF is an essential mitogen and chemoattractant for the air sacs of the drosophila tracheal system. *Dev. Cell* **3**, 195-207.
Sato, M., Kitada, Y. and Tabata, T. (2008). Larval cells become imaginal cells under the control of homothorax prior to metamorphosis in the Drosophila tracheal system. *Dev. Biol.* **318**, 247-257.
Sutherland, D., Samakovlis, C. and Krasnow, M. A. (1996). branchless encodes a Drosophila FGF homolog that controls tracheal cell migration and the pattern of branching. *Cell* **87**, 1091-1101.
Tanaka-Matakatsu, M., Uemura, T., Oda, H., Takeichi, M. and Hayashi, S. (1996). Cadherin-mediated cell adhesion and cell motility in Drosophila trachea regulated by the transcription factor Escargot. *Development* **122**, 3697-3705.
Uv, A., Cantera, R. and Samakovlis, C. (2003). Drosophila tracheal morphogenesis: intricate cellular solutions to basic plumbing problems. *Trends Cell Biol.* **13**, 301-309.
Weaver, M. and Krasnow, M. A. (2008). Dual origin of tissue-specific progenitor cells in Drosophila tracheal remodeling. *Science* **321**, 1496-1499.
Weiss, A., Charbonnier, E., Ellertsdottir, E., Tsirigos, A., Wolf, C., Schuh, R., Pyrowolakis, G. and Affolter, M. (2010). A conserved activation element in BMP signaling during Drosophila development. *Nat. Struct. Mol. Biol.* **17**, 69-76.